

Abundance determination from global emission-line SDSS spectra: exploring objects with high N/O ratios

L.S. Pilyugin^{1,2}, J.M. Vílchez², L. Mattsson³, T.X. Thuan⁴

¹ Main Astronomical Observatory of National Academy of Sciences of Ukraine, 27 Zabolotnogo str., 03680 Kiev, Ukraine

² Instituto de Astrofísica de Andalucía, CSIC, Apdo, 3004, 18080 Granada, Spain

³ Dark Cosmology Centre, Niels Bohr Institute, University of Copenhagen, Juliane Maries Vej 30, DK-2100, Copenhagen Ø, Denmark

⁴ Astronomy Department, University of Virginia, P.O. Box 400325, Charlottesville, VA 22904-4325, USA

Accepted 2011 December 20. Received 2011 December 19; in original form 2011 November 17

ABSTRACT

We have compared the oxygen and nitrogen abundances derived from global emission-line SDSS spectra of galaxies using (1) the T_e method and (2) two recent strong line calibrations: the ON and NS calibrations. Using the T_e method, anomalously high N/O abundances ratios have been found in some SDSS galaxies. To investigate this, we have Monte Carlo simulated the global spectra of composite nebulae by a mix of spectra of individual components, based on spectra of well-studied H II regions in nearby galaxies. We found that the T_e method results in an underestimated oxygen abundance (and hence in an overestimated nitrogen-to-oxygen ratio) if H II regions with different physical properties contribute to the global spectrum of composite nebulae. This effect is somewhat similar to the small-scale temperature fluctuations in H II regions discussed by Peimbert. Our work thus suggests that the high T_e -based N/O abundances ratios found in SDSS galaxies may not be real. However, such an effect is not expected to be present in dwarf galaxies since they have generally an uniform chemical composition. The ON and NS calibrations give O and N abundances in composite nebulae which agree with the mean luminosity-weighted abundances of their components to within ~ 0.2 dex.

Key words: galaxies: abundances – ISM: abundances – H II regions

1 INTRODUCTION

Metallicities play a key role in many studies of galaxies. Gas-phase oxygen and nitrogen abundances are broadly used to estimate these metallicities. It is believed (e.g. Stasińska 2006) that emission lines in spectra of H II regions are the most powerful indicators of the chemical composition of galaxies, both in the low- and intermediate-redshift universe. The spectra of a large number of individual H II regions in nearby spiral and irregular galaxies have now been obtained (McCall, Rybski & Shields 1985; Zaritsky, Kennicutt & Huchra 1994; van Zee et al. 1998; van Zee & Haynes 2006; Bresolin, Kennicutt, & Garnett 1999; Bresolin et al. 2005, 2009, among many others). These spectroscopic measurements provide basis for investigations of metallicity properties (such as radial abundance gradients, central metallicities, etc) of galaxies (Zaritsky, Kennicutt & Huchra 1994; van Zee et al. 1998; Bresolin, Kennicutt, & Garnett 1999; Pilyugin, Vílchez, & Contini 2004b, among others).

Kennicutt (1992) pioneered another method of spectral investigation of galaxies, considering the global, i.e. spatially unresolved, spectrophotometry of a sample of 90 galaxies spanning the entire Hubble sequence. In recent years, the number of available spectra of emission-line nebulae has increased dramatically

due to the completion of several large spectral surveys such as the Sloan Digital Sky Survey (SDSS, York et al. 2000). Measurements of emission lines in SDSS spectra have been used for abundance determinations in a number of studies (Kníazev et al. 2004; Izotov et al. 2006; Tremonti et al. 2004; Asari et al. 2007; Thuan et al. 2010, among others). The auroral lines are measurable in a relatively large number of SDSS galaxies (Kníazev et al. 2004; Izotov et al. 2006) that provide the possibility to obtain T_e -based abundances for SDSS galaxies.

The SDSS spectra are obtained through 3-arcsec diameter fibers. At a redshift of $z = 0.025$, the projected aperture diameter is ~ 1.5 kpc, while it is ~ 10 kpc at a redshift of $z = 0.17$. This suggests that SDSS spectra of distant galaxies are closer to global spectra of galaxies, i.e. they are the integrated spectra of multiple rather than just one H II region. Therefore the meaning of T_e -based abundances in SDSS galaxies is unclear. If a single giant H II region, excited by a single star cluster, is responsible for the global SDSS spectrum then one can expect that the T_e -based abundance to be a good estimate of the true one. Such a situation occurs only in nearby SDSS galaxies and in some distant SDSS galaxies where a single supergiant H II region, resulting from a strong starburst, makes a dominant contribution to the global spectrum. One can ex-

pect, however, that in a majority of distant SDSS galaxies, multiple individual H II regions contribute to the global spectrum.

Ercolano et al. (2007, 2010) have investigated the effect of multiple ionization sources in H II regions on the total elemental abundances derived from the analysis of collisionally excited emission lines. They considered the case of an ionizing set composed of two stellar populations with masses of $37 M_{\odot}$ and $56 M_{\odot}$. They have shown that the temperature structures of models with centrally concentrated ionizing sources can be quite different from those of models where the ionizing sources are randomly distributed within the volume, with generally non-overlapping Strömgren spheres. Since the SDSS composite nebula can be ionised by sources of different temperatures then the meaning of the measured electron temperature in distant SDSS galaxies and consequently, that of the T_e -based abundance is not evident.

This problem is in some sense similar to the one concerning the validity of the T_e -based abundances in H II regions with small-scale temperature fluctuations (Peimbert 1967) or/and with large variations of the electron temperature across the nebula (Stasińska 1978, 2005). According to Peimbert, since the line fluxes in the spectrum of such a nebula are weighted in favor of the hot regions, the electron temperature estimated from the auroral-to-nebular lines ratio will be overestimated and the abundance underestimated. While the existence of such temperature fluctuations in individual H II regions is still debated, temperature variations of individual H II regions within a composite nebula are to be perfectly natural. Thus, such an effect is probably at work in the distant SDSS galaxies.

When the electron temperature of an extragalactic H II region cannot be measured, then its location in some emission-line diagrams is used for estimating its oxygen abundance. This approach to abundance determination in H II regions, proposed by Pagel et al. (1979) and Alloin et al. (1979), is usually referred to as the “strong line method”. Numerous relations have been proposed to convert metallicity-sensitive emission-line ratios into metallicity or temperature estimates (e.g. Dopita & Evans 1986; Zaritsky, Kennicutt & Huchra 1994; Vilchez & Esteban 1996; Pilyugin 2000, 2001; Denicolo, Terlevich & Terlevich 2002; Pettini & Pagel 2004; Tremonti et al. 2004; Pilyugin & Thuan 2005; Liang et al. 2006; Stasińska 2006; Bresolin 2007; Pérez-Montero & Contini 2009; Thuan et al. 2010). Although SDSS spectra of distant galaxies are closer to global galaxy spectra than to spectra of individual H II regions, abundances in distant SDSS galaxies have been estimated using the strong line methods developed for abundance determination in individual H II regions (Tremonti et al. 2004; Erb et al. 2006; Asari et al. 2007; Thuan et al. 2010, among others). This, despite the warning of Stasińska (2010) that the strong line methods should be used only for nebulae having the same structural properties as those of the calibration samples.

However, there is a reason to expect the calibrations may provide more robust abundances in composite nebulae than the T_e method. For definiteness, we will discuss the case of oxygen abundances. The auroral and nebular lines originate in transitions from levels that differ significantly in energy, with the levels that give rise to the auroral line being at higher energies than those for nebular lines. Therefore, the emissivity of the auroral line depends much more strongly on the electron temperature in the nebula than that of the nebular line. Hence, the auroral and nebular line fluxes in the integrated spectra of composite nebulae are weighted in different ways: the hot regions will give relatively more weight to the auroral line than to the nebular lines. This means the nebular and auroral lines in the spectra of composite nebulae correspond to dif-

ferent temperatures, i.e. they are not self-consistent. The electron temperature estimated from the auroral-to-nebular lines ratio will then be overestimated and the abundance will be underestimated (Peimbert 1967; Stasińska 1978, 2005). In the case of the empirical calibrations considered here (the ON and NS calibrations), combinations of strong lines for different ions serve as abundance and electron temperature indicators. The differences between the energies of parent levels for these nebular lines are smaller than those between the energies of parent levels for the auroral and nebular lines. Then one can expect that, in the strong line method, the different regions will give roughly similar relative contributions to the nebular line fluxes, i.e. they will all correspond to more or less similar electron temperatures. This, in turn, will result in more robust global abundances estimates.

The goal of the present study is to examine to what extent abundances for distant SDSS galaxies derived in different ways (by the classic T_e method and through recent calibrations) agree or disagree. The abundances of a sample of SDSS galaxies are examined in Section 2. In Section 3, we compare the data with artificial global spectra of composite nebulae generated by Monte Carlo techniques as mixes of spectra of individual components, using spectra of real H II regions in nearby galaxies with measured electron temperatures. The meaning of abundances derived in composite nebulae in different ways and their locations in the O/H – N/O diagram are examined. A discussion of the results is given in Section 4. Section 5 presents the conclusions.

Throughout the paper, we will be using the following standard notations for the line intensities:

$$R = I_{[\text{O III}]\lambda 4363} / I_{\text{H}\beta},$$

$$R_2 = I_{[\text{O II}]\lambda 3727 + \lambda 3729} / I_{\text{H}\beta},$$

$$N_2 = I_{[\text{N II}]\lambda 6548 + \lambda 6584} / I_{\text{H}\beta},$$

$$S_2 = I_{[\text{S II}]\lambda 6717 + \lambda 6731} / I_{\text{H}\beta},$$

$$R_3 = I_{[\text{O III}]\lambda 4959 + \lambda 5007} / I_{\text{H}\beta}.$$

The electron temperatures will be given in units of 10^4K .

2 OXYGEN AND NITROGEN ABUNDANCES

2.1 Galaxy samples

2.1.1 SDSS galaxies

In our previous work (Pilyugin et al. 2010a), we have constructed a sample of galaxies by selecting from Data Release 6 of the SDSS the galaxy spectra which satisfy the following criteria: (1) both $[\text{O III}]\lambda 4363$ and $[\text{O II}]\lambda 7320 + \lambda 7330$ auroral lines are detected; (2) the spectra have smooth line profiles. Particular attention was paid to the two auroral lines mentioned above since the accuracy of the electron temperature determination depends mainly on those emission lines; (3) the emission lines do not have a broad component. The line intensities in these spectra have been measured by fitting every line with a Gaussian profile and de-reddened in the way described in Pilyugin & Thuan (2007); Pilyugin et al. (2010a).

The wavelength range of the SDSS spectra is $3800 - 9300 \text{\AA}$. Hence, for nearby galaxies with redshift $z \lesssim 0.02$, the $[\text{O II}]\lambda 7327 + \lambda 7329$ emission line is outside that range. The absence of this line prevents determination of the oxygen abundance through the standard version of the T_e method. We thus exclude the most nearby galaxies. All galaxies in our sample have redshifts larger than ~ 0.023 , i.e. they are more distant than $\sim 100 \text{Mpc}$. We thus obtain a total sample of 281 SDSS galaxies. The upper panel of Fig. 1 shows the positions of the SDSS galaxies of our sample

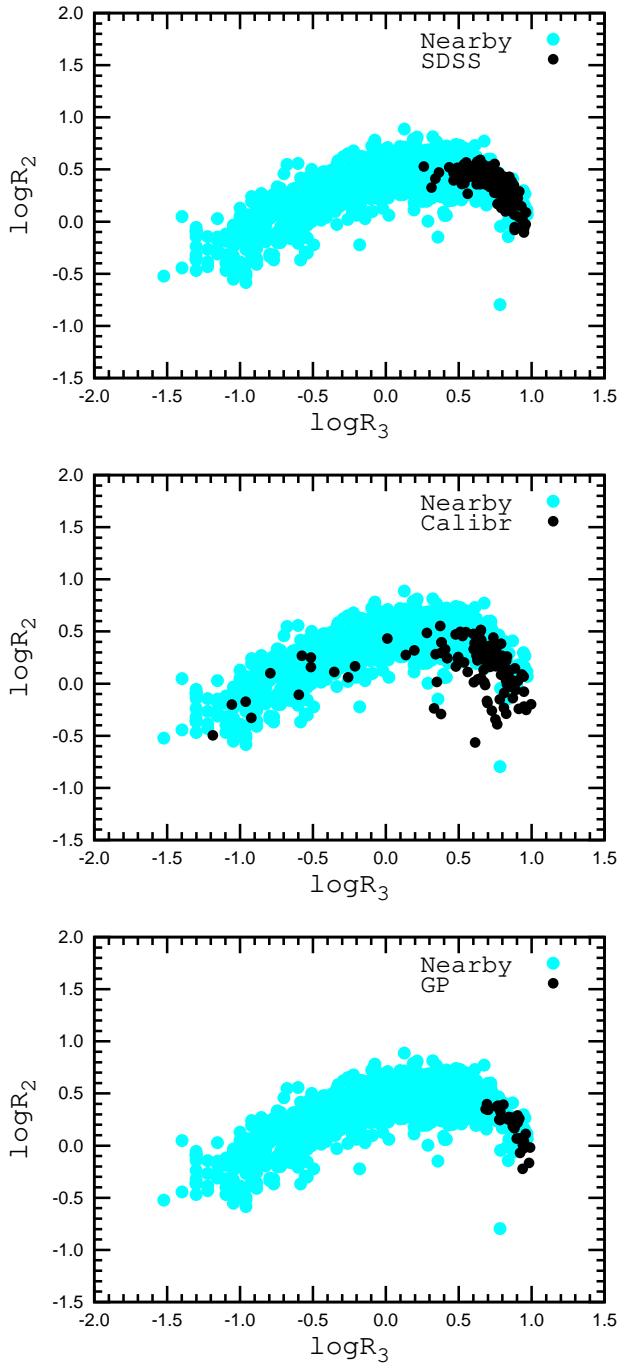


Figure 1. The $\log R_3 - \log R_2$ diagram. The filled dark (black in the color version) circles show the objects from our SDSS sample (upper panel), the sample of calibration H II regions (middle panel), and the Green Pea galaxies (lower panel). The filled grey (light-blue in the color version) circles in each panel are objects from the sample of H II regions in nearby galaxies. (A color version of this figure is available in the online version.)

in the standard $R_3 - R_2$ diagram by filled dark (black in the color version) circles.

2.1.2 H II regions in nearby galaxies

Pilyugin, Vílchez, & Contini (2004b) have made a compilation of a large amount of strong emission line measurements in spectra of

individual H II regions in nearby spiral and irregular galaxies. Their sample consists of 1121 data points and will be used to outline the area occupied by H II regions of nearby galaxies in the $R_3 - R_2$ diagram. These are shown by filled grey (light-blue in the color version) circles in the $R_3 - R_2$ diagram. Fig. 1 shows that the SDSS galaxies are located in a relatively small part of the area occupied by H II regions in nearby galaxies.

2.1.3 Calibration H II regions

The [O III] $\lambda 4363$ or/and [N II] $\lambda 5755$ auroral lines are detected in many H II regions in nearby galaxies. A compilation of such H II regions was made by Pilyugin et al. (2010b) and used as calibration data points to derive the relations which give the oxygen and nitrogen abundances and electron temperature in terms of the strong emission line fluxes. After the exclusion of a few “peculiar” objects (Pilyugin et al. 2010b), we end up with 112 data points. The spectra of this sample of H II regions in nearby spiral and irregular galaxies with detected auroral lines will be used as templates to simulate artificial spectra of composite nebulae. The middle panel of Fig. 1 shows the positions of the calibration H II regions in the $R_3 - R_2$ diagram as filled dark (black) circles. The filled grey (light-blue) circles are the same as in the upper panel.

2.1.4 Green Pea galaxies

The Green Pea galaxies have been extracted from the SDSS sample by Cardamone et al. (2009). These galaxies have a compact appearance and are characterised by distinct green colours in *gri* images. Cardamone et al. (2009) found that the Green Peas are low-mass galaxies ($M \sim 10^{8.5} - 10^{10} M_{\odot}$) with high star formation rates ($\sim 10 M_{\odot} \text{ yr}^{-1}$) with metallicities $12 + \log(\text{O}/\text{H}) \sim 8.7$. Izotov et al. (2011) have argued that they form a subset of a larger population of luminous compact star-forming galaxies. Amorín, Pérez-Montero & Vílchez (2010) have derived T_e -based oxygen abundances in these galaxies and have found that the Green Pea galaxies show metallicities $7.7 \leq 12 + \log(\text{O}/\text{H}) \leq 8.4$, with a mean value of 8.05 ± 0.14 . They have also found that some Green Pea galaxies display enhanced N/O ratios. Izotov et al. (2011) have found that the oxygen abundances $12 + \log(\text{O}/\text{H})$ in luminous compact star-forming galaxies are in the range $7.6 - 8.4$. They found no appreciable difference in element abundances between luminous compact star-forming galaxies and local blue compact dwarf galaxies, implying a similar chemical enrichment history.

From the sample of Green Pea galaxies of Cardamone et al. (2009) we have selected those with detectable [O III] $\lambda 4363$ auroral lines. The line fluxes in the SDSS spectra were measured with IRAF¹. The measured line fluxes were dereddened in the way described in Pilyugin & Thuan (2007); Pilyugin et al. (2010a). The lower panel of Fig. 1 shows the positions of the Green Pea galaxies in the $\log R_3 - \log R_2$ diagram (filled dark (black) circles). The filled grey (light-blue) circles are the same as in the upper panel. Note that the Green Pea galaxies overlap with the area occupied by our SDSS sample in the $R_3 - R_2$ diagram.

¹ IRAF is distributed by National Optical Astronomical Observatories, which are operated by the Association of Universities for Research in Astronomy, Inc., under cooperative agreement with the National Science Foundation.

2.2 Abundance determination

Line fluxes are converted to electron temperatures and ion abundances within using the standard H II region model with two distinct temperature zones within the nebula: the electron temperatures t_2 within the O⁺ zone and t_3 within the O⁺⁺ zone. Electron temperatures and ion abundances from line fluxes were derived as according to Pilyugin et al. (2010b). The ratio of the nebular to auroral oxygen line intensities $[\text{O III}]\lambda 4959 + \lambda 5007/[\text{O III}]\lambda 4363$ is used for the t_3 determination and the ratio of the nebular to auroral nitrogen line intensities $[\text{N II}]\lambda 6548 + \lambda 6584/[\text{N II}]\lambda 5755$ is used for the t_2 determination.

When only one of the electron temperatures is known, it is common practice to estimate the other temperature by using a relation between t_2 and t_3 . We have adopted the following t_2 – t_3 relation

$$t_2 = 0.672 t_3 + 0.314. \quad (1)$$

This relation derived by Pilyugin et al. (2009) is very similar to the widely used one proposed by Campbell, Terlevich & Melnick (1986) and confirmed by Garnett (1992). In general, using the classic T_e method, one can derive the oxygen abundance in each H II region in several ways: $(\text{O}/\text{H})_{t_3}$ abundances can be determined with the measured t_3 , t_2 being then estimated from the t_2 – t_3 relation; or $(\text{O}/\text{H})_{t_2}$ abundances can be found with a measured t_2 , t_3 being then estimated from the t_2 – t_3 relation. If the line-flux measurements are accurate enough, the oxygen abundances derived in these two ways should agree. The $(\text{O}/\text{H})_{t_3}$ abundance will be considered here and will be referred to as $(\text{O}/\text{H})_{T_e}$ hereafter.

We also estimate the oxygen and nitrogen abundances using two recent empirical calibrations. The ON-calibration relations give the oxygen and nitrogen abundances and electron temperature in terms of the fluxes of the strong emission lines O⁺⁺, O⁺, and N⁺. It has been derived using spectra of H II regions with well-measured electron temperatures as calibration datapoints (Pilyugin et al. 2010b). The oxygen and nitrogen abundances estimated using the ON calibration will be referred to below as $(\text{O}/\text{H})_{\text{ON}}$ and $(\text{N}/\text{H})_{\text{ON}}$.

In addition to the direct method and the ON-calibration, the NS-calibration is used as well to estimate oxygen and nitrogen abundances. These relations give abundances and electron temperatures in terms of the fluxes in the strong emission lines of O⁺⁺, N⁺, and S⁺, and have also been derived using spectra of H II regions with well-measured electron temperatures as calibration datapoints (Pilyugin & Mattsson 2011). The oxygen and nitrogen abundances estimated using the NS calibration will be referred to below as $(\text{O}/\text{H})_{\text{NS}}$ and $(\text{N}/\text{H})_{\text{NS}}$.

2.3 The O/H – N/O diagram

Fig. 2 shows a standard O/H – N/O diagram for the calibration H II regions. Using these data, we have obtained the following linear relations between $\log \text{N/O}$ and $\log \text{O/H}$

$$\begin{aligned} \log (\text{N/O}) &= -1.493 \\ &\text{for } 12 + \log (\text{O/H}) < 8.14, \\ &= 1.489 \times (12 + \log (\text{O/H})) - 13.613 \\ &\text{for } 12 + \log (\text{O/H}) > 8.14. \end{aligned} \quad (2)$$

Several H II regions show large (>0.25 dex) abundance deviations. These have been excluded in deriving the final relation. In Fig. 2, the data points used in the derivation of the final relation (102 out of 112) are shown by filled circles, while the rejected data points

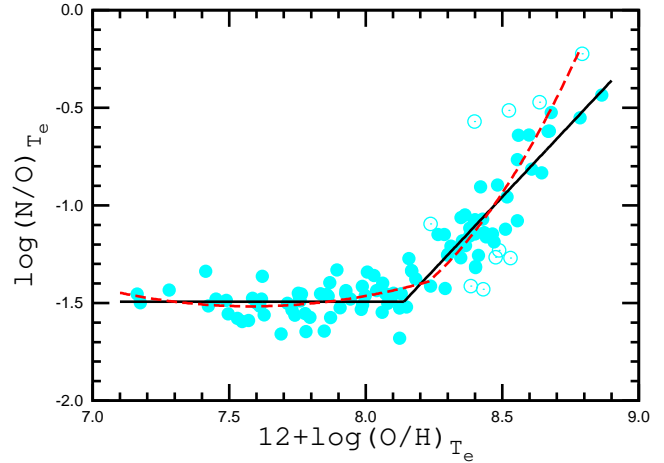


Figure 2. The O/H – N/O diagram for the calibration H II regions. The solid (black) line shows a linear fit to the N/O – O/H relation (Eq. 2). The filled circles are data points used in deriving this relation, the open circles are rejected data points. The dashed (red) line shows an alternative quadratic fit to the N/O – O/H relation.

are shown by open circles. The solid (black) line shows the derived relation. An alternate quadratic relation between $\log \text{N/O}$ and $\log \text{O/H}$ has also been derived:

$$\begin{aligned} \log (\text{N/O}) &= -1.39 + 0.39 (Z - Z_0) + 0.30 (Z - Z_0)^2 \\ &\text{for } Z < 8.23, \\ &= -1.39 + 1.24 (Z - Z_0) + 1.63 (Z - Z_0)^2 \\ &\text{for } Z > 8.23, \end{aligned} \quad (3)$$

where $Z = 12 + \log(\text{O/H})$ and $Z_0 = 8.23$ (see the dashed (red) line in Fig. 2). The two relations are similar for metallicities $12 + \log(\text{O/H}) \lesssim 8.5$. We will here only consider objects in this metallicity range. Using the N/O – O/H relationship, one can estimate the N/O ratio which corresponds to a given oxygen abundance. The nitrogen-to-oxygen abundance ratio obtained in this way will be referred to as $(\text{N/O})_{\text{REL}}$ below. For definiteness, we will use the N/O – O/H relationship given by Eq. 2.

We have derived $(\text{O}/\text{H})_{T_e}$, $(\text{O}/\text{H})_{\text{ON}}$, $(\text{O}/\text{H})_{\text{NS}}$ oxygen abundances and $(\text{N}/\text{H})_{T_e}$, $(\text{N}/\text{H})_{\text{ON}}$, and $(\text{N}/\text{H})_{\text{NS}}$ nitrogen abundances for all calibration H II regions, SDSS and Green Pea galaxies. Fig. 3 shows the comparison between O/H – N/O diagrams for abundances computed in different ways.

The upper panel of Fig. 3 shows the O/H – N/O diagram for SDSS objects (filled dark (black) circles), Green Pea galaxies (dark (red) plus signs), and calibration H II regions (filled grey (light-blue) circles) for abundances obtained with the T_e method. The upper panel shows that some SDSS objects deviate significantly from the general trend defined by the calibration H II regions: they are shifted towards higher N/O abundances ratio or/and towards lower O/H abundances. The same shift is observed for some Green Pea galaxies, in agreement with the findings of Amorín, Pérez-Montero & Vílchez (2010).

The middle panel of Fig. 3 shows the same O/H – N/O diagram, but for the case where abundances are obtained with the ON calibration, and shows that the SDSS and Green Pea galaxies follow the trend defined by the calibration H II regions, without large deviations. The lower panel of Fig. 3 shows the NS calibration-based abundances. Again, the SDSS and Green Pea galaxies follow the

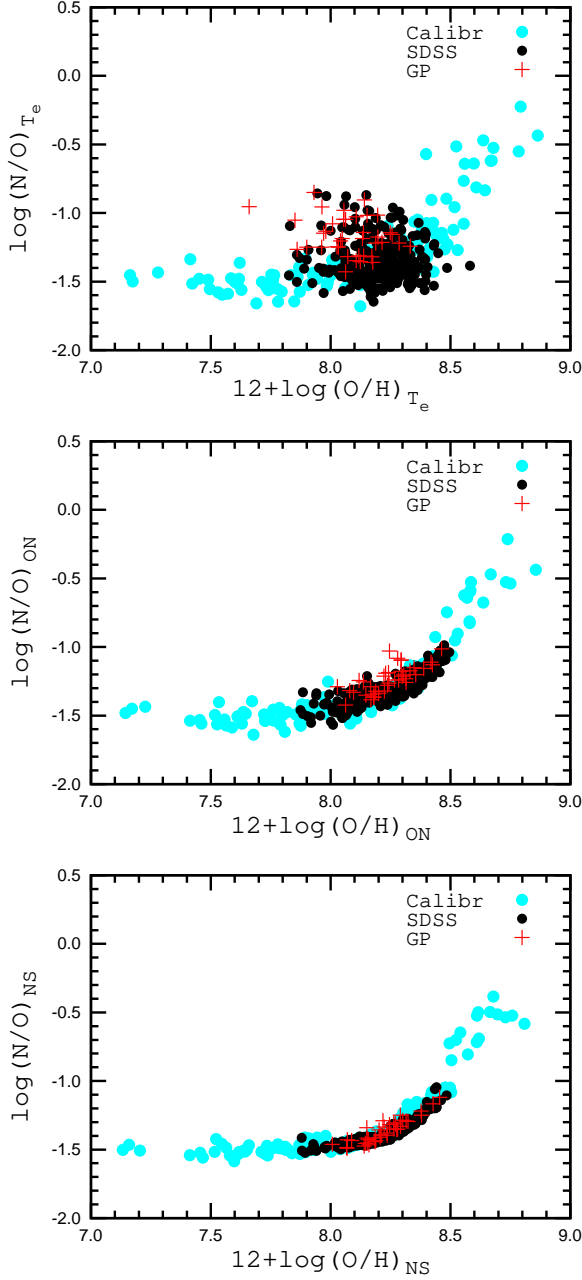


Figure 3. The O/H – N/O diagrams for SDSS objects (filled dark (black) circles), for the Green Pea galaxies (dark (red) plus signs), and for calibration H II regions (filled grey (light-blue) circles) with abundances obtained with the T_e method (upper panel), using the ON calibration (middle panel), and the NS calibration (lower panel). (A color version of this figure is available in the online version.)

trend defined by the calibration H II regions and do not show large deviations.

The upper panel of Fig. 4 shows the deviation of the $(N/O)_{T_e}$ ratio in the SDSS objects from the N/O – O/H relation as a function of the difference between T_e -based and ON-calibration-based oxygen abundances. There is a clear anti-correlation between $(\log(N/O)_{T_e} - \log(N/O)_{REL})$ and $(\log(O/H)_{T_e} - \log(O/H)_{ON})$ values. This anti-correlation suggests the deviation of SDSS objects from the general N/O – O/H trend in the upper panel of Fig. 3 is mainly

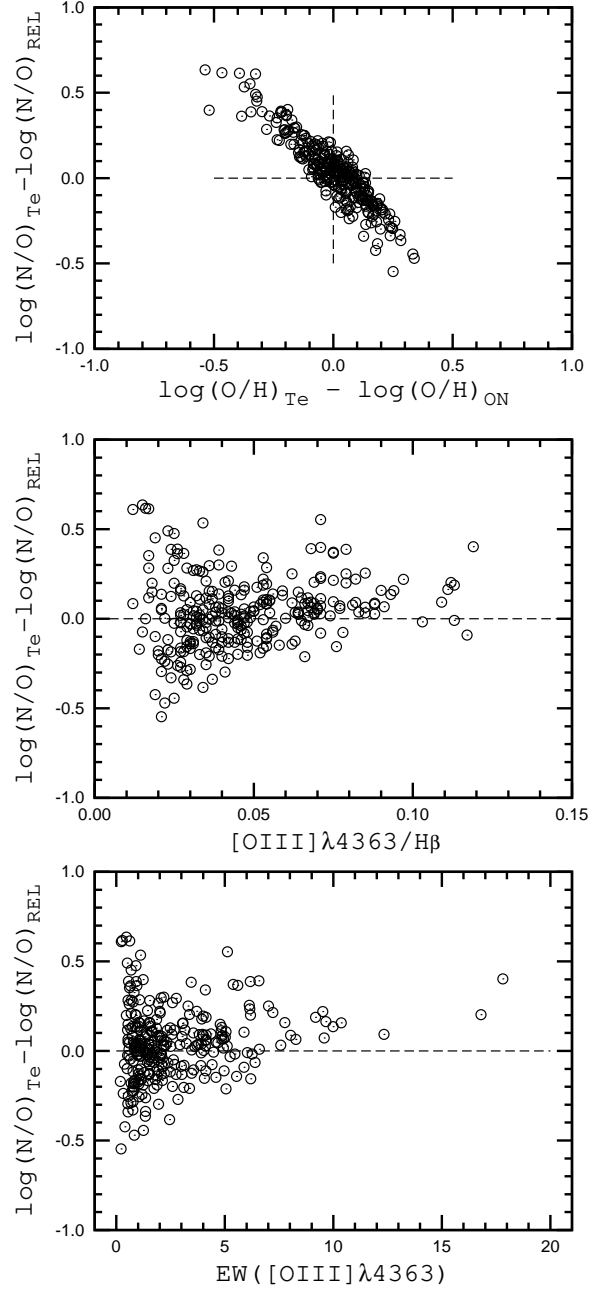


Figure 4. The deviation of the N/O ratios in SDSS objects relative the N/O – O/H relation as a function of (1) the difference between T_e -based and ON-calibration-based oxygen abundances (upper panel), (2) of the flux in the auroral line $[O III] \lambda 4363$ normalised to the H β line flux (middle panel), and (3) of the equivalent width $EW([O III] \lambda 4363)$ of the auroral line (lower panel).

caused by shifts towards lower O/H abundances, i.e. the $(O/H)_{T_e}$ abundances in these objects appear to be underestimated.

One may expect the high $(N/O)_{T_e}$ ratios in SDSS objects to be caused by uncertainties in the flux of the weak auroral $[O III] \lambda 4363$ line in these objects. To check this hypothesis, we show in the middle panel of Fig. 4 the deviation of $(N/O)_{T_e}$ ratios $(\log(N/O)_{T_e} - \log(N/O)_{REL})$ versus the flux of the $[O III] \lambda 4363$ auroral line, normalised to the H β flux. The lower panel of Fig. 4 shows the deviation of the same $(N/O)_{T_e}$ ratios as a function of the equivalent width $EW([O III] \lambda 4363)$ of the $[O III] \lambda 4363$ auroral line. Examination of

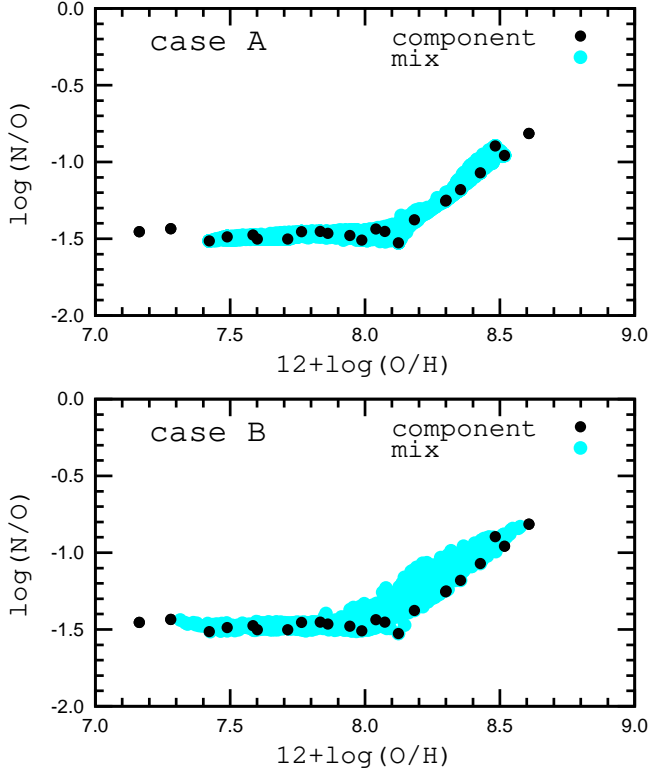


Figure 5. The O/H – N/O diagram for artificial composite nebulae and components. *Upper panel.* Filled dark (black) circles show the T_e -based abundances of components, while the grey (light-blue) filled circles are abundances of artificial composite nebulae, calculated as the mean luminosity-weighted abundance of all components, for case A. *Lower panel.* The same as in the upper panel, but for case B. (A color version of this figure is available in the online version.)

these two panels suggests that the uncertainties in the $\text{O III } \lambda 4363$ line flux can indeed be responsible for a significant fraction of high $(\text{N/O})_{T_e}$ ratios in the SDSS galaxies. However, high $(\text{N/O})_{T_e}$ ratios are found not only in SDSS objects with a weak $\text{O III } \lambda 4363$ line, but also in some objects where that line is relatively strong, with $\text{EW}(\text{O III } \lambda 4363) > 5$ and/or $\text{O III } \lambda 4363/\text{H}\beta > 0.05$. This implies that the auroral line flux uncertainties cannot be the only reason for the high $(\text{N/O})_{T_e}$ ratios found in some SDSS objects.

We propose here another explanation for the derived high $(\text{N/O})_{T_e}$ ratios. SDSS galaxies are composite nebulae which contain a number of H II regions with different physical properties, all contributing to the global spectrum. In that case, the meaning of a single measured electron temperature for the whole galaxy is not well defined and consequently, T_e -based abundances are ambiguous. We expect the electron temperature estimated from the auroral-to-nebular lines ratio to be overestimated and the derived oxygen abundance to be underestimated. In other words, such nebulae will exhibit an effect similar to the temperature fluctuations discussed by Peimbert (1967). However, these temperature variations will not occur within a single H II region, but on the large scale, in ongoing from one H II region to other. These temperature variations in an object will cause it to deviate from the general N/O – O/H trend. To explore this scenario quantitatively, we use a Monte Carlo simulation to construct spectra of composite nebulae (described in the next section), and examine how derived abundances in composite nebulae change, depending on the abundance determination method.

3 GLOBAL ABUNDANCES IN ARTIFICIAL COMPOSITE NEBULAE

3.1 Monte Carlo simulation of global spectra

To clarify the reason for the discrepancy between the T_e -based and calibration-based abundances in our sample of distant SDSS galaxies, we have simulated their spectra. We have remarked above that several different H II regions can contribute to the global spectra of distant SDSS galaxies. We have modelled their global spectra by using the approach of Pilyugin, Contini, & Vílchez (2004a); Pilyugin et al. (2010a). The artificial spectra of SDSS galaxies have been computed as a mix of spectra of individual components, which we take to be spectra of real H II regions in nearby galaxies with measured electron temperatures, taken from the calibration H II region sample.

The auroral line $\text{O III } \lambda 4363$ is usually detected in spectra of low-metallicity calibration H II regions and t_3 can then be determined, while the auroral line $\text{N II } \lambda 5755$ is detected in spectra of high-metallicity calibration H II regions, resulting in the determination of t_2 . When $\text{N II } \lambda 5755$ is detected in the spectrum of an H II region, then the intensity of $\text{O III } \lambda 4363$ is estimated in the following manner. We calculate t_3 from the measured t_2 using the $t_2 - t_3$ relation. We then estimate the line flux of $\text{O III } \lambda 4363$ corresponding to the obtained value of t_3 .

Using the calibration H II regions as components, we have performed a variety of Monte Carlo simulations, producing in each run an artificial spectrum of a composite nebula. The calibration H II regions are not distributed uniformly within the considered metallicity range. We have thus divided the metallicity range in bins of $\Delta(\log(\text{O/H})) = 0.05$ and selected one calibration H II region within each bin according to the following two criteria:

- (i) The average value of the difference between the calibration-based and T_e -based abundances is minimum. Both oxygen and nitrogen abundances and both ON and NS calibrations were taken into account in determining the average value of the difference.
- (ii) The deviation of N/O abundances ratio from the N/O – O/H relation is not in excess of 0.15 dex.

Fig. 5 shows the positions of the selected calibration H II regions in the O/H – N/O diagram by dark (black) filled circles.

At a fixed $12+\log(\text{O/H})_0$, we have simulated 100 global spectra, using the spectra of selected calibration H II regions with oxygen abundances within $12+\log(\text{O/H})_0 \pm \Delta(\log(\text{O/H}))$. The contribution from each component to a given global spectrum of artificial composite H II regions is defined by the value w_j , where w_j are random numbers between -1 and 1. To take into account that some components may not contribute to a given spectrum we choose the interval of random numbers between -1 and 1 instead of the standard interval between 0 and 1 and when $w_j < 0$ we set it to 0, i.e. the component does not make contribution to the global spectrum. The component (calibration H II region) line fluxes are given on a scale where $F(\text{H}\beta) = 1$, therefore we can consider that the value w_j defines $\text{H}\beta$ flux (or luminosity) of j component in the given variant of the global spectra. Then the total $F(\text{H}\beta)$ flux of the composite nebula is given by the expression:

$$F(\text{H}\beta) = \sum_{j=1}^{j=n} w_j, \quad (4)$$

where n is the number of components in the composite nebula.

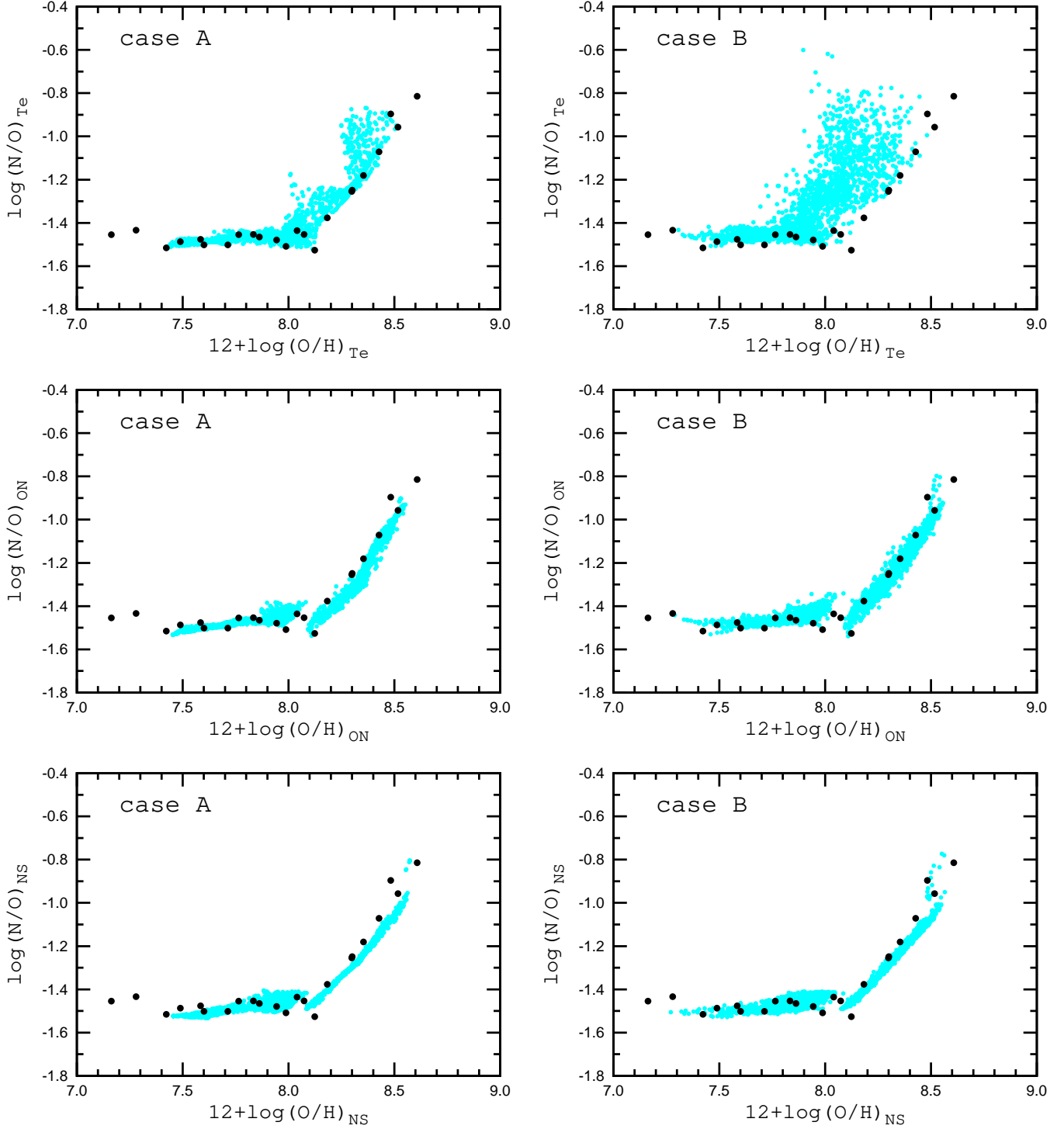


Figure 6. The O/H – N/O diagrams for the artificial composite nebulae for case A (left panels) and for case B (right panels). The grey (light-blue) filled circles show the abundances derived in different ways from artificial global spectra. The dark (black) filled circles are T_e -based abundances in the components. (A color version of this figure is available in the online version.)

The flux $F(X_{\lambda_k})$ of the composite nebula in the line X_{λ_k} is given by:

$$F(X_{\lambda_k}) = \frac{\sum_{j=1}^{j=n} w_j F_j(X_{\lambda_k})}{\sum_{j=1}^{j=n} w_j}. \quad (5)$$

We have computed the intensity of the $H\beta$, $[\text{O II}]\lambda 3727$, $[\text{O III}]\lambda 4363$, $[\text{O III}]\lambda 4959$, $[\text{O III}]\lambda 5007$, $[\text{N II}]\lambda 6548$, $[\text{N II}]\lambda 6584$, $[\text{S II}]\lambda 6717$, and $[\text{S II}]\lambda 6731$ lines for the each artificial spectrum of composite nebulae.

The mean oxygen abundance of a composite H II region, weighted by the $H\beta$ line luminosity, can be determined as

$$(\text{O}/\text{H})_{\text{mean}} = \frac{\sum_{j=1}^{j=n} w_j (\text{O}/\text{H})_j}{\sum_{j=1}^{j=n} w_j}. \quad (6)$$

Similarly, the mean nitrogen abundance in a composite H II region is given by

$$(\text{N}/\text{H})_{\text{mean}} = \frac{\sum_{j=1}^{j=n} w_j (\text{N}/\text{H})_j}{\sum_{j=1}^{j=n} w_j}. \quad (7)$$

For each computed spectrum, we have estimated t_3 , $(\text{O}/\text{H})_{\text{mean}}$, $(\text{N}/\text{H})_{\text{mean}}$, $(\text{O}/\text{H})_{T_e}$, $(\text{N}/\text{H})_{T_e}$, $(\text{O}/\text{H})_{\text{NS}}$, $(\text{N}/\text{H})_{\text{NS}}$, $(\text{O}/\text{H})_{\text{ON}}$ and $(\text{N}/\text{H})_{\text{ON}}$ abundances. This procedure was repeated for a variety of $12+\log(\text{O}/\text{H})_0$ values.

3.2 Global abundances in artificial composite nebulae

Here, we discuss two cases, represented by two sets of Monte Carlo simulations:

A. We simulated 100 global spectra for each $12+\log(\text{O}/\text{H})_0$, using components with oxygen abundances within $12+\log(\text{O}/\text{H})_0 \pm 0.15$, and varying $12+\log(\text{O}/\text{H})_0$ from 7.5 to 8.5 in steps of 0.05 dex. The grey (light-blue) filled circles in the upper panel of Fig. 5 show the mean abundances of the artificial composite nebulae for case A. The abundances of each component has been weighted by the corresponding H β -luminosities.

B. We simulated 100 global spectra for each $12+\log(\text{O}/\text{H})_0$, using components with oxygen abundances within $12+\log(\text{O}/\text{H})_0 \pm 0.35$. The grey (light-blue) filled circles in the lower panel of Fig. 5 show the mean abundances in artificial composite nebulae for case B.

The N/O – O/H diagrams for case A with abundances obtained in different ways from the global spectra are shown in the left panels of Fig. 6 by grey (light-blue) filled circles. The upper panel shows the T_e -based abundances, the middle panel the ON-calibration-based abundances, and the lower panel the NS-calibration-based abundances in the artificial composite nebulae. The dark (black) filled circles in each panel are the T_e -based abundances of each component. The upper left panel shows that a significant fraction of the artificial composite nebulae with T_e -based abundances are shifted from the O/H – N/O relation towards higher N/O ratios or/and towards lower oxygen abundances.

The left upper panel of Fig. 7 shows the difference between nitrogen-to-oxygen ratios $(\text{N}/\text{O})_{T_e}$ and $(\text{N}/\text{O})_{\text{mean}}$ in the artificial composite nebulae as a function of the difference between oxygen abundances $(\text{O}/\text{H})_{T_e}$ and $(\text{O}/\text{H})_{\text{mean}}$ for case A by the grey (light-blue) filled circles. The dark (black) filled circles show the components. The right upper panel of Fig. 7 shows the deviation of $(\text{N}/\text{O})_{T_e}$ ratios in the artificial composite nebulae from the N/O – O/H relation (the linear fit discussed previously) as a function of the difference between the oxygen abundance derived by the T_e method from global spectra and that obtained as the H β -luminosity-weighted mean abundances of components for case A.

The N/O – O/H diagram of T_e -based abundances for artificial composite nebulae for case B is shown in the upper right panel of Fig. 6 by the dark (black) filled circles. The grey (light-blue) filled circles are T_e -based abundances of the components. Again, a fraction of artificial composite nebulae with T_e -based abundances

are shifted from the O/H – N/O relation towards higher N/O ratios or/and towards lower oxygen abundances. The grey (light-blue) filled circles in the lower left panel of Fig. 7 shows the difference between nitrogen-to-oxygen ratios $(\text{N}/\text{O})_{T_e}$ and $(\text{N}/\text{O})_{\text{mean}}$ in artificial composite nebulae as a function of the difference between oxygen abundances $(\text{O}/\text{H})_{T_e}$ and $(\text{O}/\text{H})_{\text{mean}}$ for case B. The dark (black) filled circles show the individual components. The lower right panel of Fig. 7 shows the deviations of $(\text{N}/\text{O})_{T_e}$ ratios in the artificial composite nebulae from the N/O – O/H relation (the linear fit discussed previously) as a function of the difference between the oxygen abundance derived by the T_e method from global spectra and that obtained as the H β -luminosity-weighted mean abundances of components for case B.

By comparison of Fig. 4 and Fig. 7 it is evident that artificial composite nebulae reproduce the anti-correlation between $(\log(\text{N}/\text{O})_{T_e} - \log(\text{N}/\text{O})_{\text{REL}})$ and $(\log(\text{O}/\text{H})_{T_e} - \log(\text{O}/\text{H})_{\text{ON}})$ observed in our sample of SDSS galaxies. This can be considered in favour of our hypothesis that the enhanced $(\text{N}/\text{O})_{T_e}$ ratio derived for some SDSS objects can be due to the fact that these objects are composite nebulae, with a number of H II regions with different physical properties contributing to the global spectrum. Hence, the electron temperature determined from the auroral-to-nebular lines ratio is overestimated, and the oxygen abundance is underestimated in such a nebula, i.e., it appears to be a Peimbert temperature fluctuation effect (see the introduction).

The middle and lower panels of Fig. 6 show that both the ON and NS calibration-based abundances in the artificial composite nebulae follow, in general, the abundances of the components. However, both case A and B show a gap near $12+\log(\text{O}/\text{H}) \sim 8.1$. This gap is due to a transition between two regimes in the calibrations, i.e., by the fact that both “warm” and “hot” H II regions (according to the classification in Pilyugin et al. 2010b)) make contributions to the global spectrum of composite nebulae. Therefore, such composite H II regions are neither purely warm nor purely hot. But distinct calibration relations for warm and hot H II regions were in fact used (Pilyugin et al. 2010b; Pilyugin & Mattsson 2011). Hence, there appears to be a problem regarding how these calibration relations should be applied to such nebulae. It should also be noted that the criterion for distinguishing between warm and hot H II regions is somewhat arbitrary.

We have performed a variety of Monte Carlo simulations, using different sets of components and different $\Delta(\log(\text{O}/\text{H}))$ intervals, to produce artificial global spectra. We have found that the underestimation of the oxygen abundance with the T_e method – and, consequently, the shift of the position in the N/O – O/H diagram of the artificial composite nebula with T_e -based abundances relative to its position with mean oxygen and nitrogen abundances – is larger for nebulae where the components have large differences in physical properties. In particular, the value of the shift increases with increasing $\Delta(\log(\text{O}/\text{H}))$. Thus, we have reached the following conclusions:

- If the composite nebula consists of H II regions with similar physical properties or a single H II region which makes a dominant contribution to the global spectrum, then the oxygen and nitrogen abundances derived with the T_e method and the ON and NS calibrations are in satisfactory agreement with each other, and near the mean H β luminosity weighted oxygen and nitrogen abundances of the components in the composite nebula.

- If H II regions with different physical properties make comparable contributions to the global spectrum of the composite nebula,

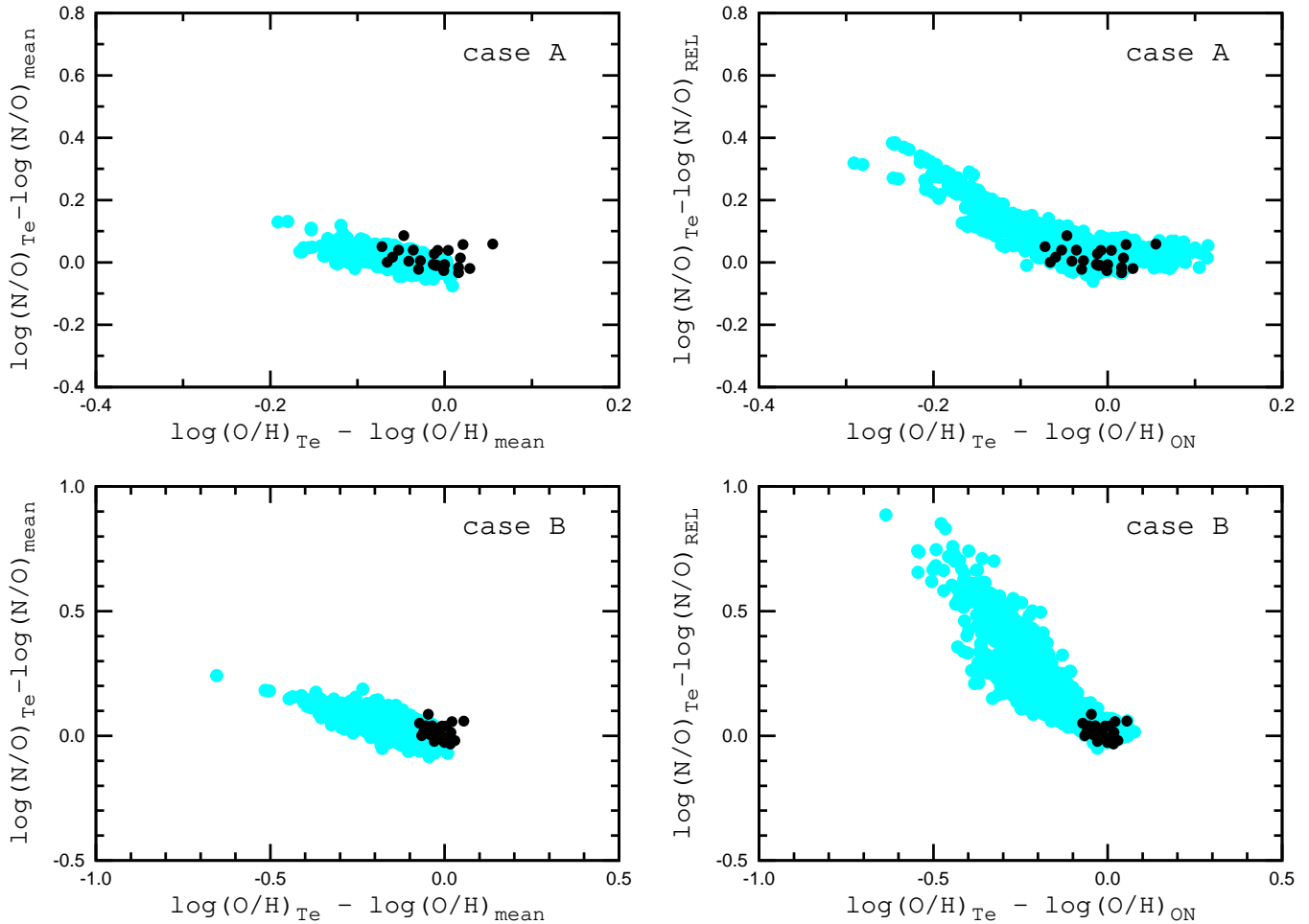


Figure 7. *Left upper panel.* The grey (light-blue) filled circles show the difference between nitrogen-to-oxygen ratios $(N/O)_{Te}$ and $(N/O)_{mean}$ in artificial composite nebulae as a function of the difference between oxygen abundances $(O/H)_{Te} - (O/H)_{mean}$ for case A. The dark (black) filled circles show the components. *Right upper panel.* The grey (light-blue) filled circles show the deviation of $(N/O)_{Te}$ ratios in artificial composite nebulae from the expected $N/O - O/H$ relation as a function of the difference between oxygen abundances derived with the T_e method from global spectra and those obtained through ON calibration. *Lower panels* show the same but for case B. (A color version of this figure is available in the online version.)

then the T_e - based oxygen abundance can be underestimated. Hence, the position of such a nebula in the $N/O - O/H$ diagram will be shifted towards lower oxygen abundances, mimicking an enhancement of the N/O ratio.

- The ON and NS calibrations give oxygen and nitrogen abundances in the composite nebulae which agree with the mean luminosity-weighted abundances of their components to within ~ 0.2 dex.

It should be noted that the high-metallicity ($12 + \log(O/H) \geq 8.5$) calibration H II regions with measured electron temperatures are very few. Thus, they cannot be simulated and we cannot investigate how similar (or dissimilar) their abundances estimated using the T_e method and the strong-line calibrations are. Furthermore, our approach does not allow to take into account the contribution of a diffuse emission.

4 DISCUSSION

Our conclusion that the global abundances derived for composite nebulae with the classic T_e method may be subject to systematic

errors is not surprising. First, an effect of this kind has been predicted by Peimbert (1967) for H II regions with a non-uniform electron temperature. Second, Kobulnicky et al. (1999) have compared physical conditions derived from spectroscopy of individual H II regions with those obtained from global spectroscopy for several galaxies with $12 + \log(O/H) \sim 8.2$, and where the auroral line $[O III] \lambda 4363$ is detected in both individual and global spectra. They found that the standard T_e method using global spectra give systematic errors in that the oxygen abundances derived from global spectra are systematically 0.05 – 0.2 dex below the median values computed from spectra obtained in smaller apertures.

The global oxygen abundances estimated with the one-dimensional R_{23} calibration have been discussed by Kobulnicky et al. (1999); Moustakas & Kennicutt (2006), while those obtained with the two dimensional R_{23} calibration (P method) have been discussed by Pilyugin, Contini, & Vílchez (2004a). It has been found that the abundance inferred from the integrated emission-line spectrum of a galaxy using one- or two-dimensional R_{23} calibrations is representative of the gas-phase oxygen abundance at a fixed galactocentric radius (equal to 0.4 times the isophotal radius), as determined by the abundance gradient derived from H II regions. Here, we have found that the

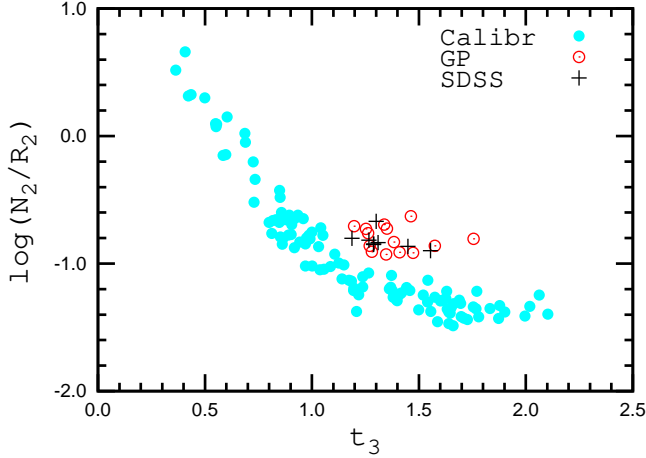


Figure 8. The flux ratio N_2/R_2 as a function of electron temperature t_3 . The grey (light-blue) filled circles show the calibration H II regions. The SDSS objects with large (> 0.3 dex) deviations from the expected N/O – O/H relation are shown by dark (black) plus signs. The Green Pea galaxies with large deviations from the expected N/O – O/H relation are shown by open (red) circles. (A color version of this figure is available in the online version.)

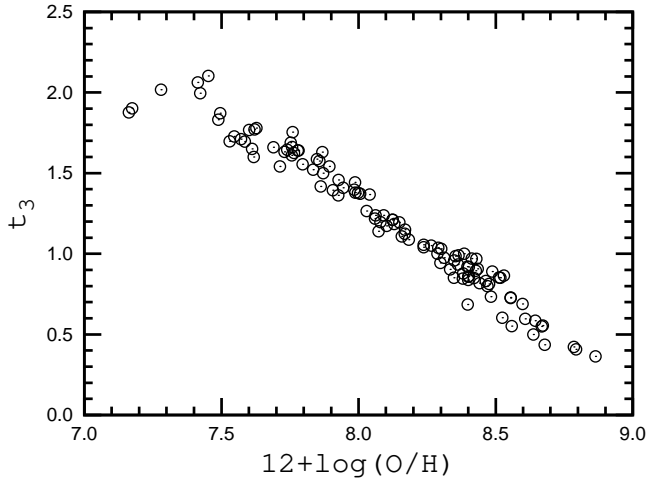


Figure 9. Electron temperature t_3 as a function of oxygen abundance for the calibration H II regions.

global abundances derived using the ON and NS calibrations are close to the mean abundances. Thus, the calibrations produce robust global abundances although both the absolute values of abundances in individual H II regions and of global abundances depend on the adopted calibration.

Our results suggest the T_e -based abundances in some composite nebulae can be incorrect and shift the positions of these nebulae in the O/H – N/O diagram towards higher N/O abundances ratio or/and towards lower O/H abundances relatively to the positions of H II regions in nearby galaxies. Thus the high $(N/O)_{T_e}$ abundances ratios obtained in some SDSS and Green Pea galaxies may be incorrect because they are composite nebulae.

Fig. 8 shows the N_2/R_2 flux ratios as a function of the electron temperature t_3 for the calibration H II regions and for the SDSS and Green Pea galaxies with large (> 0.3 dex) deviations from the expected N/O – O/H relation. In the ON calibration, the N_2/R_2 flux ratios are used as temperature indicators. Fig. 8 shows that the measured N_2/R_2 in SDSS and Green Pea galax-

ies with $t_3 \sim 1.4$ have values that are more typical for nebulae with $t_3 \sim 1$. This means the two electron temperature indicators ($[\text{O III}]\lambda 4959, \lambda 5007/[\text{O III}]\lambda 4363$ and N_2/R_2) are in conflict. Thus, to reproduce both the measured electron temperature t_3 and the N_2/R_2 flux ratios, the composite nebula should contain a component with a temperature $t_3 \sim 1$ as well as one with $t_3 \gtrsim 1.4$. The temperature difference between components can be larger than 5000 K, in some cases. For example, the hottest Green Pea galaxy in our sample (with a large N/O deviation), J012910.15 + 145934.6, has $t_3 = 1.75$ while its measured N_2/R_2 flux ratio is typical for a nebula with $t_3 \sim 1$.

Fig. 9 shows t_3 as a function of the oxygen abundance $12+\log(\text{O}/\text{H})$ for the calibration H II regions. We see that a H II region with $t_3 \sim 1$ has $12+\log(\text{O}/\text{H}) \sim 8.3$. Can a hot component of metallicity $12+\log(\text{O}/\text{H}) \sim 8.3$ be responsible for the high t_3 value (~ 1.4) in the composite nebula?

We can expect the points in the t_3 – O/H diagram (Fig. 9) to be close to the highest attainable electron temperatures t_3 for a given $12+\log(\text{O}/\text{H})$ because of a selection effect: electron temperatures are easiest to measure in the hottest H II regions. In such case, an H II region of metallicity $\log(\text{O}/\text{H}) = 8.3$ cannot have an electron temperature as high as $t_3 \sim 1.4$. Thus, a hot component with $12+\log(\text{O}/\text{H}) \sim 8.3$ cannot be responsible for the high electron temperature measured.

According to Fig. 9, a H II region with $t_3 \sim 1.4$ has $12+\log(\text{O}/\text{H}) \sim 8.0$. Furthermore, the N_2/R_2 flux ratio increases with decreasing electron temperature. Can a cold component with $12+\log(\text{O}/\text{H}) \sim 8.0$ be responsible for the high N_2/R_2 ?

The typical N/O ratio in H II regions with $\log(\text{O}/\text{H}) \sim 8.0$ is $\log(\text{N}/\text{O}) \sim -1.5$. A H II region with $\log(\text{O}/\text{H}) \sim 8.0$ and $\log(\text{N}/\text{O}) = -1.5$ would have $\log N_2/R_2 = -0.9$ at $t_3 \sim 0.5$. However, the line fluxes N_2 and R_2 (normalised to the $\text{H}\beta$ flux) are one order of magnitude lower than the measured fluxes. Thus, a cold component of metallicity $12+\log(\text{O}/\text{H}) \sim 8.0$ cannot be responsible for the high N_2/R_2 flux ratio measured.

The measured high N/O ratios and high electron temperatures in some SDSS and Green Pea galaxies can be reproduced by composite nebulae involving components of different metallicities. However, the metallicity difference can be as large as a factor 2-3, or even larger in extreme cases. It is believed that Green Peas are low-mass galaxies (Cardamone et al. 2009; Amorín, Pérez-Montero & Vílchez 2010; Izotov et al. 2011). The metallicity scatter of H II regions in typical dwarf galaxies is known to be small (e.g. Croxall et al. 2009). This suggests that the measured high N/O ratios not in all the Green Pea galaxies can be reproduced by composite nebulae and some Green Pea galaxies may not be typical dwarfs galaxies. A large metallicity scatter of the H II regions in a dwarf galaxy can arise if this galaxy has undergone an atypical evolution. For example, it can be the result of the merging of two dwarfs of different metallicities, triggering a starburst in both components simultaneously. Infall of non-enriched gas onto a well-evolved galaxy with a high N/O gas-phase ratio would decrease the oxygen and nitrogen abundances, and would result in a galaxy with an enhanced N/O ratio. The evolution of a galaxy with selective heavy elements loss through enriched galactic winds can also result in enhanced N/O ratios (e.g. Pilyugin 1993; Yin, Matteucci, & Vladilo 2011).

5 CONCLUSIONS

We have examined the oxygen and nitrogen abundances derived from global emission-line spectra of galaxies with $12 + \log(\text{O}/\text{H})$ ranging from ~ 7.5 to ~ 8.5 , based on a sample of 281 SDSS galaxies with measured electron temperatures. The oxygen and nitrogen abundances in these galaxies were derived with the T_e method as well as with two recent strong-line calibrations: the ON and NS calibrations.

For T_e -based abundances, the positions of some SDSS galaxies in the O/H – N/O diagram are shifted towards higher N/O ratios or/and towards lower O/H abundances relative to the positions of H II regions in nearby galaxies. In case of strong-line calibration-based abundances, the SDSS galaxies occupy the same area in the O/H – N/O diagram as the H II regions in nearby galaxies.

The global spectra of galaxies have been Monte Carlo simulated as a mix of spectra of individual components, based on well-observed H II regions in nearby galaxies. Abundance analysis of the artificial composite nebulae yields the following conclusions:

(i) If the composite nebula consists of H II regions with similar physical properties or a single H II region makes a dominant contribution to the global spectrum, then the oxygen and nitrogen abundances derived with the T_e method and the ON and NS calibrations are in satisfactory agreement with each other and near the mean H β luminosity weighted value of oxygen and nitrogen abundances of the individual components of the composite nebula.

(ii) If H II regions with different physical properties make comparable contributions to the global spectrum, then the T_e - based oxygen abundances may be underestimated and the position of such a nebula in the N/O – O/H diagram will be shifted towards lower oxygen abundances, mimicking an enhancement of the N/O ratio in the nebula. This effect is similar to the one discussed by Peimbert for H II regions with small scale temperature fluctuations. For composite nebulae however, this effect appears to be due to temperature variations on large spatial scales, caused by varying temperatures in different components of the composite nebula.

(iii) The ON and NS calibrations give oxygen and nitrogen abundances in composite nebulae which agree with the mean luminosity-weighted abundances of their components to within ~ 0.2 dex. ON- and NS-calibration-based abundances for these nebulae also show a gap in abundance near $12 + \log(\text{O}/\text{H}) \sim 8.1$.

(iv) The high (N/O) $_e$ ratios derived in some Green Pea galaxies may be caused by the fact that their SDSS spectra are spectra of composite nebulae made up of several components with different physical properties (such as metallicity). However, for the hottest Green Pea galaxies, which appear to be dwarf galaxies, this explanation does not seem to be plausible. It would work only if the H II regions in these galaxies have a dispersion of abundances much larger than that typically found in dwarf galaxies.

ACKNOWLEDGEMENTS

We are grateful to the referee for his/her constructive comments. L.S.P. acknowledges support from the Cosmomicrophysics project of the National Academy of Sciences of Ukraine. J.M.V. and L.S.P. acknowledge the partial support of AYA2010-21887-C04-01 from the Spanish PNAYA and CSD2006-00070 from CONSOLIDER 2010 programme of MICINN. L.S.P. thanks the hospitality of the Instituto de Astrofísica de Andalucía where this investigation was carried out. The Dark Cosmology Centre is funded by the Danish National Research Foundation.

Funding for the SDSS and SDSS-II has been provided by the Alfred P. Sloan Foundation, the Participating Institutions, the National Science Foundation, the U.S. Department of Energy, the National Aeronautics and Space Administration, the Japanese Monbukagakusho, the Max Planck Society, and the Higher Education Funding Council for England. The SDSS Web Site is <http://www.sdss.org/>.

The SDSS is managed by the Astrophysical Research Consortium for the Participating Institutions. The Participating Institutions are the American Museum of Natural History, Astrophysical Institute Potsdam, University of Basel, University of Cambridge, Case Western Reserve University, University of Chicago, Drexel University, Fermilab, the Institute for Advanced Study, the Japan Participation Group, Johns Hopkins University, the Joint Institute for Nuclear Astrophysics, the Kavli Institute for Particle Astrophysics and Cosmology, the Korean Scientist Group, the Chinese Academy of Sciences (LAMOST), Los Alamos National Laboratory, the Max-Planck-Institute for Astronomy (MPIA), the Max-Planck-Institute for Astrophysics (MPA), New Mexico State University, Ohio State University, University of Pittsburgh, University of Portsmouth, Princeton University, the United States Naval Observatory, and the University of Washington.

REFERENCES

- Alloin D., Collin-Souffrin S., Joly M., Vigroux L., 1979, A&A, 78, 200
- Amorín R.O., Pérez-Montero E., Vílchez J.M., 2010, ApJ, 715, L128
- Asari N.V., Cid Fernandes R., Stasińska G., Torres-Papaqui J.P., Mateus A., Sodré L., Schoenell W., 2007, MNRAS, 381, 263
- Bresolin F., Kennicutt R.C., Jr., Garnett D.R., 1999, ApJ, 510, 104
- Bresolin F., Shaerer D., González Delgado R.M., Stasińska G., 2005, A&A, 441, 981
- Bresolin F., 2007, ApJ, 656, 186
- Bresolin F., Gieren W., Kudritzki R.-P., Pietrzyński G., Urbaneja M.A., Carraro G., 2009, ApJ, 700, 309
- Campbell A., Terlevich R., Melnick J., 1986, MNRAS, 223, 811
- Cardamone C., Schawinski K., Sarzi M., et al., 2009, MNRAS, 399, 1191
- Croxall K.V., van Zee L., Lee H., Skillman E.D., Lee J.C., Côté S., Kennicutt R.C., Jr. Miller B.W., 2009, ApJ, 705, 723
- Denicolo G., Terlevich R., Terlevich E., 2002, MNRAS, 330, 69
- Dopita M.A., Evans I.N., 1986, ApJ, 307, 431
- Erb D.K., Shapley A.E., Pettini M., Steidel C.C., Reddy N.A., Adelberger K.L., 2006, ApJ, 644, 813
- Ercolano B., Bastian N., Stasińska G., 2007, MNRAS, 379, 945
- Ercolano B., Wesson R., & Bastian N. 2010, MNRAS, 401, 1375
- Garnett D.R. 1992, AJ, 103, 1330
- Izotov Y.I., Stasińska G., Meynet G., Guseva N.G., Thuan T.X., 2006, A&A, 448, 955
- Izotov Y.I., Guseva N.G., Thuan T.X., 2011, ApJ, 728, 161
- Kennicutt R.C., (Jr.), 1992, ApJ, 338, 310
- Kniazev A.Y., Pustilnik S.A., Grebel E.K., Lee H., Pramskij A.G., 2004, ApJS, 153, 429
- Kobulnicky H.A., Kennicutt R.C., (Jr.), Pizagno J.L., 1999, ApJ, 514, 544
- Liang Y.C., Yin S.Y., Hammer F., Deng L.C., Flores H., Zhang B., 2006, ApJ, 652, 257
- McCall M.L., Rybski P.M., Shields G.A., 1985, ApJS, 57, 1
- Moustakas J., Kennicutt R.C., (Jr), 2006, ApJ, 651, 155

- Pagel B.E.J., Edmunds M.G., Blackwell D.E., Chun M.S., Smith G., 1979, MNRAS, 189, 95
 Peimbert M., 1967, ApJ, 150, 825
 Pettini M., Pagel B.E.J., 2004, MNRAS, 348, 59L
 Pérez-Montero E., Contini T., 2009, MNRAS, 398, 949
 Pilyugin L.S., 1993, A&A, 277, 42
 Pilyugin L.S., 2000, A&A, 362, 325
 Pilyugin L.S., 2001, A&A, 369, 594
 Pilyugin L.S., Contini T., Vílchez J.M., 2004a, A&A, 423, 427
 Pilyugin L.S., Vílchez J.M., Contini T., 2004b, A&A, 425, 849
 Pilyugin L.S., Thuan T.X., 2005, ApJ, 631, 231
 Pilyugin L.S., Thuan T.X., 2007, ApJ, 669, 290
 Pilyugin L.S., Mattsson L., Vílchez J.M., Cedrés B., 2009, MNRAS, 398, 485
 Pilyugin L.S., Vílchez J.M., Cedrés B., & Thuan T.X. 2010a, MNRAS, 403, 896
 Pilyugin L.S., Vílchez J.M., Thuan T.X., 2010b, ApJ, 720, 1738
 Pilyugin L.S., Mattsson L., 2011, MNRAS, 412, 1145
 Stasińska G., 1978, A&A, 66, 257
 Stasińska G., 2005, A&A, 434, 507
 Stasińska G., 2006, A&A, 454, L127
 Stasińska G., 2010, Proceedings of the IAU Sump. No 262, 93
 Thuan T.X., Pilyugin L.S., Zinchenko I.A., 2010, ApJ, 712, 1029
 Tremonti C.A., Heckman T.M., Kauffmann G., et al., 2004, ApJ, 613, 898
 van Zee L., Haynes M.P., 2006, ApJ, 636, 214
 van Zee L., Salzer J.J., Haynes M.P., O'Donoghue A.A., Balonek T.J., 1998, AJ, 116, 2805
 Vílchez J.M., Esteban C., 1996, MNRAS, 280, 720
 Yin J., Matteucci F., Vladilo G., 2011, A&A, 531, A136
 York D.G., Anderson J.E., Anderson S.F., et al., 2000, AJ, 120, 1579
 Zaritsky D., Kennicutt R.C., Huchra J.P., 1994, ApJ, 420, 87